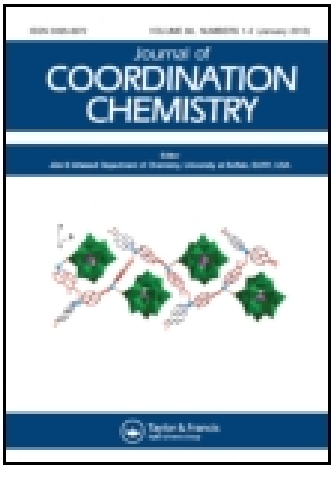

Journal of Coordination Chemistry
Publication details, including instructions for authors and subscription information:
http://www.tandfonline.com/loi/gcoo20

Synthesis, characterization, interactions with DNA and bovine serum albumin (BSA), and antibacterial activity of cyclometalated iridium(III) complexes containing dithiocarbamate derivatives

Titas Mukherjee[a], Manjira Mukherjee[a], Buddhadeb Sen[a], Snehasis Banerjee[b], Geeta Hundal[c] & Pabitra Chattopadhyay[a]

[a] Department of Chemistry, Burdwan University, Burdwan, India

[b] Department of Chemistry, Government College of Engineering and Leather Technology, Kolkata, India

[c] Department of Chemistry, Guru Nanak Dev University, Amritsar, India

Accepted author version posted online: 21 Jul 2014.Published online: 11 Aug 2014.

To cite this article: Titas Mukherjee, Manjira Mukherjee, Buddhadeb Sen, Snehasis Banerjee, Geeta Hundal & Pabitra Chattopadhyay (2014) Synthesis, characterization, interactions with DNA and bovine serum albumin (BSA), and antibacterial activity of cyclometalated iridium(III) complexes containing dithiocarbamate derivatives, Journal of Coordination Chemistry, 67:15, 2643-2660, DOI: 10.1080/00958972.2014.945924

To link to this article: http://dx.doi.org/10.1080/00958972.2014.945924

Journal of Coordination Chemistry, 2014
Vol. 67, No. 15, 2643–2660, http://dx.doi.org/10.1080/00958972.2014.945924

Synthesis, characterization, interactions with DNA and bovine serum albumin (BSA), and antibacterial activity of cyclometalated iridium(III) complexes containing dithiocarbamate derivatives

TITAS MUKHERJEE†, MANJIRA MUKHERJEE†, BUDDHADEB SEN†, SNEHASIS BANERJEE‡, GEETA HUNDAL§ and PABITRA CHATTOPADHYAY*†

†Department of Chemistry, Burdwan University, Burdwan, India
‡Department of Chemistry, Government College of Engineering and Leather Technology, Kolkata, India
§Department of Chemistry, Guru Nanak Dev University, Amritsar, India

(*Received 1 March 2014; accepted 4 June 2014*)

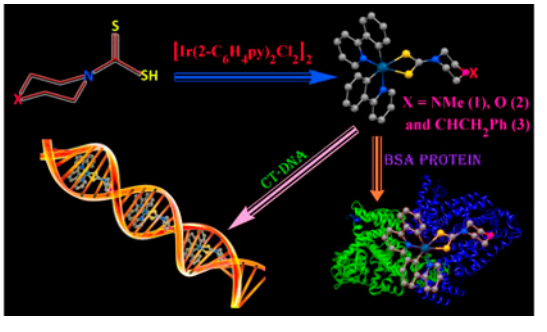

Three mononuclear cyclometalated iridium(III) complexes having dithiocarbamate ligands, [Ir^{III}(2-$C_6H_4py)_2$(L)] (where 2-C_6H_4py = 2-phenylpyridine; and $\mathbf{L^1H}$ = 4-MePipzcdtH, $\mathbf{L^2H}$ = MorphcdtH, and $\mathbf{L^3H}$ = 4-BzPipercdtH for **1**, **2**, and **3**, respectively), were synthesized from [Ir(2-$C_6H_4py)_2Cl]_2 \cdot 1/4CH_2Cl_2$ by displacing the two bridging chlorides with one dithiocarbamate ligand. The complexes were characterized using physicochemical and spectroscopic tools along with structural analysis of [Ir(2-$C_6H_4py)_2(L^2)$] (**2**) by single crystal X-ray diffraction. Structural analysis of **2** showed a distorted octahedron in which the nitrogen donor of one 2-phenylpyridine and the carbon donor of another 2-phenylpyridine are in axial positions, *trans* to one another. Electrochemical analysis by cyclic voltammetry showed the irreversible two-electron equivalent reduction voltammograms of **1**, **2**, and **3** attributable to Ir(III) to Ir(I). Electronic characterizations of these complexes are consistent with significant delocalization of the sulfur electron density onto the empty metal d-orbital. The intercalative interaction of the complexes with calf thymus DNA was evaluated using absorption, fluorescence quenching, and viscosity measurements. The binding affinities of these complexes with bovine serum albumin were estimated in terms of quenching constants using the Stern–Volmer equation. Study of antibacterial activities of the complexes by agar disk diffusion against some species of pathogenic bacteria was also performed.

*Corresponding author. Email: pabitracc@yahoo.com

Keywords: Iridium(III) complex; Dithiocarbamates; Crystal structure; Redox behavior with DFT; Biological study

1. Introduction

The chemistry of iridium(III) complexes is important in organic light-emitting diodes, catalysts, and anticancer agents. Iridium(III) complexes, particularly bis- and tris-cyclometalated (C^N) complexes of iridium(III) based on 2-phenylquinoline and its derivatives, have been widely used as promising electroluminescent materials for OLED technology because cyclometalated iridium(III) complexes having a d^6-electron configuration show strong spin-orbit coupling, efficient intersystem crossing from the singlet excited state to the triplet manifold, and enhancement of the T_1-S_0 transition, displaying efficient phosphorescent emission at room temperature [1–10]. Several reports on the evolution of selective recognition for Hg^{2+} with multi-signaling optical–electrochemical response by introducing sulfur to these cyclometalated ligands are also in the literature [11–17] compared to the reports of biological applications of iridium(III) complexes [18–28]. Among these biological applications, DNA-binding studies have been a focus to explore the intercalation characteristics of iridium(III) complexes into DNA in quest of relatively inert iridium-based anticancer complexes of higher potency, higher cancer cell selectivity, lower resistance, and reduced side effects [25–28]. Study of interaction with DNA and bovine serum albumin (BSA), and antibacterial activity of cyclometalated iridium(III) complexes bearing dithiocarbamate derivatives, is still unexplored.

Dithiocarbamate ($R_2NCS_2^-$) sulfurs maintain additional coordination capability due to the availability of a pair of potentially bonding electrons, leading to applications in chemical bonding, industry, biology, and biochemistry [29–35]. The nature of the heterocycle and the metal ion attached to dithiocarbamate control the potential pharmacological and catalytic efficiency of the metal complexes [36].

Herein, an account of the syntheses, characterizations, electrochemical behaviors, and biological properties of a new series of three mononuclear cyclometalated iridium(III) complexes bearing dithiocarbamate derivatives has been described. This report deals with the chemistry of $[Ir^{III}(2\text{-}C_6H_4py)_2(SS)]$ complexes, where 2-C_6H_4py = 2-phenylpyridine and SS = 4-MePipzcdt (L^1) for **1**, Morphcdt (L^2) for **2**, and 4-BzPipercdt (L^3) for **3**. The physico-chemical and spectroscopic properties of **1**, **2**, and **3** along with the detailed structural analyses of **2** have been included. The intercalative mode of binding interactions of these complexes with calf thymus DNA (CT-DNA) have been investigated to explore the biological activity of new complexes, as pharmacological effectiveness depends on intercalative binding to DNA [37–40]. The association of **2** with BSA with spectroscopic tools has also been examined. Antibacterial activities of **1**, **2**, and **3** against *Escherichia coli*, *Vibrio cholerae*, *Streptococcus pneumoniae*, and *Bacillus cereus* have also been studied by agar disk diffusion.

2. Experimental

2.1. *Materials and physical measurements*

Iridium trichloride, 2-phenylpyridine, morpholine, and 4-benzylpiperidine (Aldrich) were purchased and used without purification. $[Ir(2\text{-}C_6H_4py)_2Cl]_2 \cdot 1/4CH_2Cl_2$ was prepared

following the reported procedure [41]. CT-DNA was obtained from Bangalore Genie, India. Solvents used for spectroscopic studies and for synthesis were purified and dried by standard procedures before use. The organic moieties, 4-methylpiperazine-l-carbodithioic acid (4-MePipzcdtH, $\mathbf{L^1H}$), morpholine-4-carbodithioic acid (MorphcdtH, $\mathbf{L^2H}$), and 4-benzylpiperidine-l-carbodithioic acid (4-BzPipercdtH, $\mathbf{L^3H}$) were obtained as solid products following our earlier report [42].

The Fourier transform infrared spectra of the ligand and complexes were recorded on a Perkin Elmer FTIR model RX1 spectrometer using KBr pellets from 4000 to 300 cm^{-1}. Solution phase electronic spectra were recorded on a JASCO UV–vis/NIR spectrophotometer model V-570 from 200 to 1100 nm. Elemental analyses were carried out on a Perkin Elmer 2400 series-II CHNS Analyzer. Steady-state fluorescence emission and excitation spectra were recorded with a Hitachi F-4500 FL spectrophotometer. Mass spectra of **1**, **2**, and **3** were recorded on Micromass Q-T of micro^{TM}. NMR spectra of the ligands and complexes have been recorded on a Bruker DPX-300. Solution conductivities were measured using a Systronics Conductivity Meter 304 model and redox potentials by CHI620D potentiometer in DMF at ~10^{-3} M L^{-1}. Stock solutions of protein (1.00×10^{-4} M L^{-1}) were prepared by dissolving BSA in 0.05 M phosphate buffer at pH 7.4 and storing at 0–4 °C in the dark. The concentration of BSA was determined from optical density measurements using molar absorptivity of $\varepsilon_{280} = 44{,}720$ M^{-1} cm^{-1} [43].

2.2. *Syntheses of [Ir(2-C_6H_4py)$_2$(L^1)] (1), [Ir(2-C_6H_4py(L^2)] (2) and [Ir(2-C_6H_4py)$_2$(L^3)] (3)*

The complexes have been synthesized with the help of a common procedure as stated below. To solution of the ligand, $\mathbf{L^1H}$ (177 mg, 1.0 mM) for **1**, or $\mathbf{L^2H}$ (164 mg, 1.0 mM) for **2**, or $\mathbf{L^3H}$ (253 mg, 1.0 mM) for **3** in DMSO-MeCN (v/v 1 : 1), the solution of [Ir(2-C_6H_4py)$_2$Cl]$_2$·1/4CH_2Cl_2 (557 mg, 0.5 mM) in acetonitrile was added. The resulting solution was refluxed under nitrogen for 12 h and the color changed from faded yellow to orange. On slow evaporation, a microcrystalline solid appeared, which was then subjected to purification by TLC on a silica plate with C_6H_6–MeCN (v/v 3 : 1) as eluent; an orange band separated, which was extracted with MeCN. Needle-shaped crystals of [Ir(2-C6H4py)$_2$(L^2)] suitable for X-ray diffraction were grown from this solution on evaporation at ambient temperature.

[Ir(2-C_6H_4py)$_2$(L^1)] (1): [$C_{28}H_{27}N_4IrS_2$]; Yield: 88%. Anal. Calcd: C, 49.76; H, 4.03; N, 8.29; S, 9.49. Found: C, 49.03; H, 3.89; N, 8.76; S, 9.11. IR (cm^{-1}): $\nu_{C=N}$, 1490; $\nu_{a(SCS)}$, 1012, 996. ESI-MS (*m/z*): [M + Na^+], 698.90(23% abundance); [M + H^+], 676.898 (59.1% abundance). Conductivity (Λ_o, M^{-1} cm^{-1}) in DMF: 42. ^{1}H NMR (δ, ppm in dmso-d_6): 4.35 (m, 3H of N–CH_3); 3.79 (m, 4H of S_2C–N(CH_2)$_2$); 3.15 (m, 4H of –N(CH_2)$_2$). Protons of 2-C_6H_4py: C_1–H (8.84, d, 2H), C_5–H (8.01, d, 2H), C_4–H (7.69, d, 2H), C_3–H (7.68, m, 2H), C_6–H, C_7–H, and C_8–H (7.43, m, 6H), C_2–H (7.27, m, 2H).

[Ir(2-C_6H_4py)$_2$(L^2)] (2): [$C_{27}H_{24}N_3OIrS_2$]; Yield: 90%. Anal. Calcd: C, 48.92; H, 3.65; N, 6.34; S, 9.67. Found: C, 48.01; H, 3.41; N, 6.97; S, 9.01. IR (cm^{-1}): $\nu_{C=N}$, 1480; $\nu_{a(SCS)}$, 1035, 1014. ESI-MS (*m/z*): [M + Na^+], 685.85 (21% abundance); [M + H^+], 663.858 (57.6% abundance). Conductivity (Λ_o, M^{-1} cm^{-1}) in DMF: 35. ^{1}H NMR (δ, ppm in dmso-d_6): 3.78–3.86 (m, 4H of S_2C–N(CH_2)$_2$); 3.65–3.67 (m, 4H of O(CH_2)$_2$). Protons of 2-C_6H_4py: C_1–H (8.86, d, 2H), C_5–H (8.00, d, 2H), C_4–H (7.69, d, 2H), C_3–H (7.67, m, 2H), C_6–H, C_7–H, and C_8–H (7.41, m, 6H), C_2–H (7.27, m, 2H).

[Ir(2-C_6H_4py)$_2$(L^3)] (3): [$C_{35}H_{32}N_3IrS_2$]; Yield: 83%. Anal. Calcd: C, 55.98; H, 4.29; N, 5.60; S, 8.54. Found: C, 55.22; H, 4.11; N, 6.10; S, 8.08. IR (cm^{-1}): $\nu_{C=N}$, 1496; $\nu_{a(SCS)}$, 1042, 1025. ESI-MS (*m/z*): [M + Na^+], 754.02 (16% abundance); [M + H^+], 752.008 (34% abundance). Conductivity (Λ_o, $M^{-1}\,cm^{-1}$) in DMF: 45. ^{1}H NMR (δ, ppm in dmso-d_6): 7.19–7.29 (m, 5H of C_6H_5); 3.91 (m, 4H of S_2C–N(CH_2)$_2$); 3.18 (t, 2H of CH_2, $j = 6.2$); 2.21 (m, 1H of CH); 1.73–1.77 (m, 4H of (CH_2)$_2$). Protons of 2-C_6H_4py: C_1–H (8.83, d, 2H), C_5–H (8.02, d, 2H), C_4–H (7.70, d, 2H), C_3–H (7.69, m, 2H), C_6–H, C_7–H, and C_8–H (7.43, m, 6H), C_2–H (7.28, m, 2H).

2.3. *X-ray crystallography*

X-ray data of a suitable crystal of **2** were collected on a Bruker Apex-II CCD diffractometer using Mo Kα ($\lambda = 0.71069$) radiation. The data were corrected for Lorentz and polarization effects, and empirical absorption corrections were applied using SADABS from Bruker. A total of 13,691 reflections were measured, out of which 4012 were independent and 2299 were observed [$I > 2\sigma(I)$] for theta (θ) 32°. The structure was solved by direct methods using SIR-92 and refined by full-matrix least squares based on F^2 using SHELX-97 [44]. The twofold axis passes through the metal ion, nitrogens of the piperazine ring and their substituent carbons. Therefore, the asymmetric unit contains half the molecule. All non-hydrogen atoms were refined anisotropically. The refinement showed rotational disorder in the piperazine ring which could be resolved by splitting the two unique carbons into two components and refining their sof and thermal parameters as free variables with restraints over the bond distances. All hydrogens were fixed geometrically with their U_{iso} values 1.2 times the phenylene and methylene carbons, and 1.5 times the methyl carbons. All calculations were performed using the Wingx package [45, 46]. Important crystallographic parameters are given in table 1.

Table 1. Crystal data and structure refinement for **2**.

Empirical formula	$C_{27}H_{24}IrN_3O_2S_2$, $0.5H_2O$
Fw	678.81
Crystal system	Triclinic
Space group	*P-1*
a (Å)	9.7183(4)
b (Å)	11.4054(5)
c (Å)	12.3144(6)
β (°)	100.737(2)
V (Å^3)	1274.16(10)
Z	2
D_{Calcd} (g cm^{-3})	1.769
μ (Mo Kα) (mm^{-1})	5.433
F (0 0 0)	664
θ Range (°)	1.77–27.00
No. of reflns. collected	19,902
No. of indep. reflns.	5488
R_{int}	0.0224
No. of reflns. ($I > 2\sigma(I)$)	5195
No. of refined parameters	316
Goodness-of-fit (F^2)	1.091
R_1, wR_2 ($I > 2\sigma(I)$)	0.0193, 0.0491
R indices (all data)	$R_1 = 0.0211$, 0.0500

2.4. *DNA-binding experiments*

All the experiments involving CT-DNA were studied by spectrophotometric titration and fluorescence quenching using ethidium bromide (EB) as a DNA scavenger in tris-buffer solution, and performing the experiment by our method [47].

Concentrated stock solution of **2** was prepared by dissolving the compound in DMSO and diluting with tris–HCl buffer to the required concentration for all experiments. Absorption spectral titration experiment was performed by keeping constant the concentration of **2** and varying the CT-DNA concentration. To eliminate the absorbance of DNA itself, equal solution of CT-DNA was added both to **2** solution and to the reference solution.

In the EB fluorescence displacement experiment, 5 μL of EB tris–HCl solution (1.0 mM L^{-1}) was added to 1.0 mL of DNA solution (at saturated binding levels), storing in the dark for 2.0 h. Then solution of the compound was titrated into the DNA/EB mixture and diluted in tris–HCl buffer to 5.0 mL to get the solution with the appropriate complex **1**/CT-DNA mole ratio. Before measurements, the mixture was shaken and incubated at room temperature for 30 min. The interaction of **2** with CT-DNA was investigated by absorption and emission spectra along with viscometric measurements to discern between DNA intercalation and groove binding.

2.5. *BSA-binding experiments*

Binding with BSA for **2** was done dissolving BSA in MilliQ water ($1.0 \times 10^{-5}\,M^{-1}$) and the stock solution of the complex was prepared in DMSO-H_2O (1 : 99 v/v) mixture at $1.0 \times 10^{-5}\,M^{-1}$ concentration. Both the absorption and fluorescence quenching experiments (λ_{ex} = 280 nm) were performed by gradually increasing the complex concentration, keeping fixed the concentration of BSA. All the experimental sets were carefully degassed purging pure nitrogen for 5 min.

2.6. *Antimicrobial screening*

The biological activities of free dithiocarbamic acids and the iridium(III) derivatives of dithiocarbamates (**1**, **2**, and **3**) have been studied for antibacterial activities by agar well diffusion method [48, 49]. The antibacterial activities were done at 100 μg/mL concentration in DMF using three pathogenic gram-negative bacteria (*E. coli*, *V. cholerae*, and *S. pneumoniae*) and one gram-positive pathogenic bacterium (*B. cereus*). DMF was used as a negative control. The Petri dishes were incubated at 37 °C for 24 h. After incubation, the plates were observed for inhibition zones. The diameter of the zone of inhibition was measured in mm.

2.7. *Theoretical calculation*

To clarify the configurations and energy levels of **1**, **2**, and **3**, DFT calculations were carried out in G09W program using B3LYP/6-31G(d) calculation and correlation function as implemented in the Gaussian program package, Gaussian 09. Thermal contribution to the energetic properties was considered at 298.15 K and one atmosphere pressure.

3. Results and discussion

3.1. *Synthesis and characterization of complexes*

L^1H, **L^2H**, and **L^3H** were synthesized by the reaction between carbon disulfide and different amines in ethanol, and later characterized by FTIR and ^1H NMR spectra. Treatment of these ligands with $[Ir(2\text{-}C_6H_4py)_2Cl]_2 \cdot 1/4CH_2Cl_2$ under refluxing conditions in DMSO-MeCN (v/v 1 : 1) having a nitrogen atmosphere resulted in cleavage of the chloro bridge and formation of mononuclear iridium(III) complexes of the general formula $[Ir^{III}(2\text{-}C_6H_4py)_2(L)]$, which were obtained from column chromatography using acetonitrile as orange microcrystalline solid on evaporation. Here, the dithiocarbamates are bidentate monobasic ligands (*viz.* scheme 1). Complexes **1–3** are sparingly soluble in organic solvents, except hexane, but fairly soluble in DMF and DMSO, and are stable in both the solid state and solution in air. Spectroscopic and elemental analyses confirm the formulations of the complexes. The molar conductivity of freshly prepared solution (~1×10^{-3} M concentration) of **1** ($\Lambda_M = 42\ M^{-1}\ cm^{-1}$), **2** ($\Lambda_M = 35\ M^{-1}\ cm^{-1}$), and **3** ($\Lambda_M = 45\ M^{-1}\ cm^{-1}$) in DMF are consistent with non-electrolytes. The magnetic susceptibility measurements are in agreement with diamagnetic complexes.

3.2. *Structural description of 2*

An ORTEP view of $[Ir(2\text{-}C_6H_4py)_2(L^2)]$ (**2**) with atom-labeling scheme is illustrated in figure 1, and the selected bond distances and angles are listed in table 2. The structural

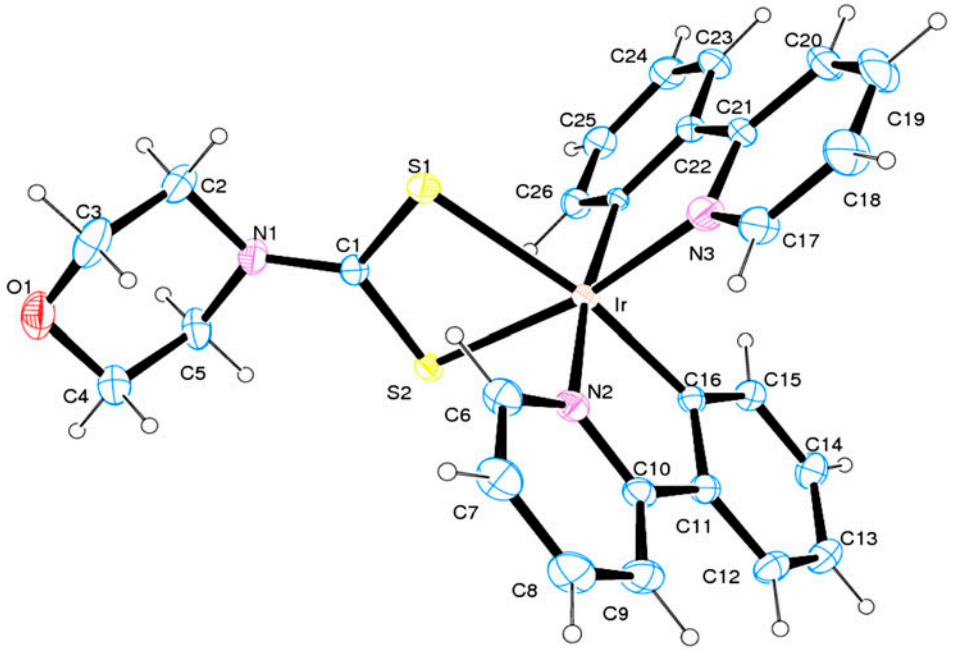

Figure 1. ORTEP view of $[Ir(2\text{-}C_6H_4py)_2(L^2)]$ (**2**) with atom-labeling scheme of the crystallographically independent part (Symmetry codes: (i) $-x, y, z$; (ii) $x, -y, -z$; (iii) $-x, -y, -z$).

Table 2. Coordination bond lengths (Å) and angles (°) for **2**.

Bond lengths (Å)			
Ir(1)–S(1)	2.490(8)	Ir(1)–N(3)	2.011(3)
Ir(1)–S(2)	2.459(7)	Ir(1)–C(16)	2.006(3)
Ir(1)–N(2)	2.047(2)	Ir(1)–C(27)	2.040(2)
Bond angles (°)			
C(27)–Ir(1)–N(3)	80.38(11)	N(2)–Ir(1)–S(1)	97.17(8)
C(27)–Ir(1)–S(1)	88.85(7)	N(3)–Ir(1)–S(1)	99.59(9)
S(1)–Ir(1)–S(2)	71.16(2)	C(27)–Ir(1)–S(2)	95.28(7)
S(2)–Ir(1)–N(2)	100.14(11)	C(27)–Ir(1)–N(2)	172.51(9)
C(16)–Ir(1)–N(2)	80.27(11)	C(16)–Ir(1)–S(1)	169.99(8)
C(16)–Ir(1)–N(3)	90.27(11)	C(16)–Ir(1)–C(27)	94.54(11)
N(3)–Ir(1)–N(2)	94.18(11)	N(3)–Ir(1)–N(2)	94.18(11)

Notes: Symmetry transformations used to generate equivalent atoms: #1 $-x+1, y, -z+3/2$.

analysis shows that **2** resides on a *P-1* site in the triclinic crystal system. The crystal structure of **2** is a distorted octahedron in which the nitrogen of one 2-phenylpyridine and the carbon donor of another 2-phenylpyridyl ligand are in axial positions. Both Ir–C σ-bonds are equal (1.994(4) Å) and significantly shorter than the Ir–N dative bond lengths of 2.039 (3) Å. The bond distance of Ir–C in **2** is comparable with the previously reported Ir–C bonds in cyclometalated complexes (1.996(9) Å), but the Ir–N bond is slightly longer than those (1.987(7) Å) [50]; both are comparable with reported values [51]. Both Ir–S distances are also equal (2.4854(11) Å) and longer than those found in $[Ir(Et_2NCS_2)_3]$ (2.364(3) Å) [51] due to the attachment of sulfur to carbon of more electronegativity than phosphorus. The S–Ir–S angle of 71.00(5)° is smaller compared to the observed value of 79.40(1)° in the previous report [51]. The structural analysis showed a highly disordered water O1 W near the inversion center; it was refined with 0.5 sof. The hydrogens attached to it were located from the difference Fourier and were initially refined with 0.5 sofs with their isotropic thermal parameters fixed as 1.2 times that of the oxygen and O–H distance at 0.84(2) Å.

3.3. *IR spectra*

The IR spectra of the ligands display intense stretches at 2850 and 1445–1430 cm^{-1} from $\nu_{C\text{-}H}$ of $\nu_{N\text{–}Me}$, and $\nu_{C=N}$, respectively. The $\nu_{C\text{–}H}$ of $\nu_{N\text{–}Me}$ of $\mathbf{L^1H}$ for **1** (2915 cm^{-1}) is blue-shifted from $\nu_{C\text{–}H}$ of $\nu_{N\text{–}Me}$ of the free ligand (2850 cm^{-1}), indicating metal ligand coordination. The band around 1500 cm^{-1} indicates double bond character of C–N bond in the ligand frame, confirmed by the X-ray structure. This could be attributed to electron releasing of the heterocyclic group towards sulfur, a feature that induces electron delocalization over the carbon–nitrogen bond and the CS_2 fragment. This is shown by the $\nu_{C=N}$ shift to higher energies (*ca.* 1480–1496 cm^{-1}) with respect to the free acids (*ca.* 1445–1430 cm^{-1}), and these bands lie between the stretching frequencies expected for a double C=N (1610–1690 cm^{-1}) and single C–N bond (1250–1350 cm^{-1}). The blueshift of the C=N stretching frequency on going from the free acids to their metal complexes gives support to the bidentate character [52] of the carbodithioic acid ligands. Two bands at 1042–996 cm^{-1} (separated by less than 20 cm^{-1}), assignable to the $\nu_{a(SCS)}$ and one band for the $\nu_{s(SCS)}$ at 708–678 cm^{-1} of the complexes, suggest unsymmetrical chelating bidentate mode of coordination to iridium(III) [53]. The stretching due to ν_{COC} (asym and sym), $\nu_{N\text{–}Me}$, and ν_{CCC} (asym and sym) remain unchanged in spectra of the complexes from the free ligands, excluding coordination to the metals via nitrogen and oxygen donors.

Table 3. UV–vis spectral data.

Compound	λ_{max} (nm) (log ε)[a]
1	435 (2.50), 390 (3.35), 359sh (3.95), 335 (3.92), 313 (3.97)
2	442 (2.60), 386 (3.35), 353sh (3.94), 314 (3.92)
3	438 (2.65), 382 (3.39), 352sh (3.90), 319 (3.96)

[a]In DMSO solvent.

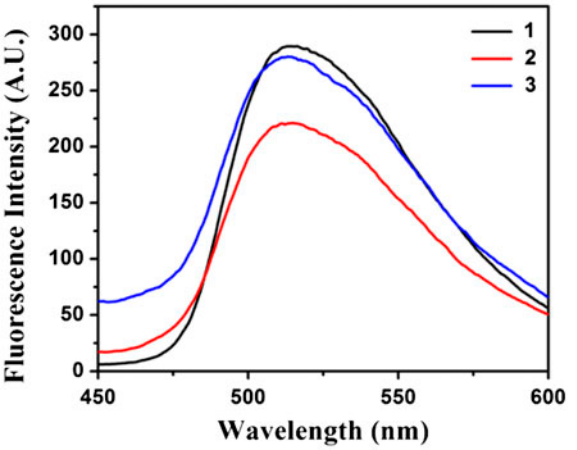

Figure 2. Emission spectra of **1**, **2**, and **3** at 10^{-5} M in deoxygenated acetonitrile solution at 298 K ($\lambda_{ex} = 364$, 340, and 313 nm for **1**, **2**, and **3**, respectively).

3.4. *Electronic and fluorescence spectra*

The electronic spectral data of **1**, **2**, and **3** in DMSO have been tabulated in table 3 (figure 2). The higher energy band at 385–390 nm for all three complexes with high extinction coefficients are due to coordinated carbon atom from piperidine moiety, C(σ)–Ir(III) charge transfer transition. The other higher energy intense transitions at 352 and 359 nm are due to $n \rightarrow \pi^*$ and $\pi \rightarrow \pi^*$ charge transfer transitions. Complexes **1**, **2**, and **3** display relatively low-energy bands at 435, 442, and 438 nm, respectively, with low extinction coefficient values assignable to spin-allowed metal-to-ligand charge transfer [dπ(Ir)$\rightarrow\pi^*$(2-C_6H_4py)]. The characteristics of these transitions are very close to the previous reports for [dπ(Ir)–π^*(bipy)] [51, 54–56].

3.5. *Redox studies*

The cyclic voltammograms (CV) of **1**, **2**, and **3** were recorded in DMF at room temperature. A three-electrode cell, platinum, Ag/AgCl, and a platinum wire as a working, reference, and auxiliary electrode, respectively, has been used for measurements. The CV of **1**, **2**, and **3** are shown in figure 3, and the electrochemical data are tabulated in table 4. The complexes exhibit an irreversible reductive response at $E_{1/2} \approx -0.766$ to -0.810 V (*versus* Ag/AgCl) corresponding to Ir^{3+}/Ir^{+} couple. Small differences in the ΔE_p values 665, 593, and 630 mV for **1**, **2**, and **3**, respectively, have been observed, increasing in the order **1** > **3** > **2**. The trend

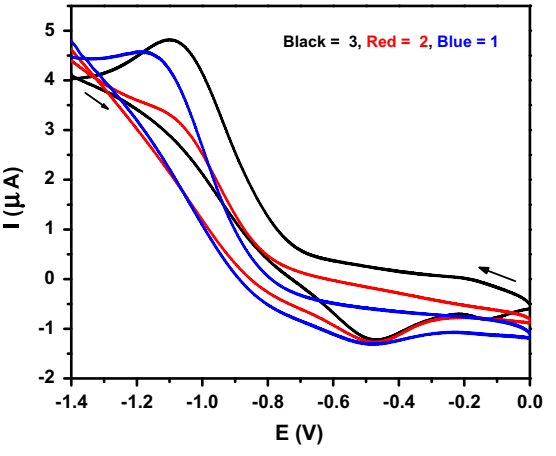

Figure 3. CV (scan rate 50 mV/s) of **1**, **2,** and **3** in DMF solution of 0.1 M TBAP using platinum working electrode. Potentials *vs.* non-aqueous Ag/AgCl.

Table 4. Electrochemical data[a] for **1**, **2**, and **3**.

Complex	E_{pc} (V)	E_{pa} (V)	ΔE_p (mV)	$E_{1/2}$ (V)
1	−1.094	−0.464	665	−0.810
2	−1.143	−0.478	593	−0.766
3	−1.063	−0.470	630	−0.779

[a]Potentials *vs.* non-aqueous Ag/Ag^+ reference electrode, scan rate 50 mV/s, supporting electrolyte: tetra-N-butylammonium perchlorate (0.1 M).

of reduction potential values can be explained by the energy level diagram for the frontier π MOs of complexes obtained from DFT calculation (*viz.* supporting information). This study supports lowest cathodic potential value for **2** (−0.766 V) in accord with the calculated LUMO of **2** is of lowest energy (LUMO (133) = −0.0473 eV), whereas the LUMO of the highest energy (LUMO (137) = −0.0443 eV) is in agreement with the highest cathodic potential (−0.810 V) for **1**.

3.6. *DNA-binding study of 2*

3.6.1. Absorption spectral study. Electronic absorption spectroscopy is an effective method to examine the binding modes of **2** with DNA. In general, binding of the compound to the DNA helix shows an increase of the CT band for **2**, due to strong intercalative interactions between an aromatic chromophore of the compound and the base pairs of DNA [57, 58]. The absorption spectra of **2** in the absence and presence of CT-DNA are given in figure 4. The extent of the hyperchromism in the absorption band is generally consistent with the strength of intercalative binding [59, 60]. Figure 5 indicates that **2** interacts strongly with CT-DNA ($K_b = 0.31 \times 10^5\ M^{-1}$), and the observed spectral changes may be rationalized in terms of intercalative binding [61]. In order to further illustrate the binding strength of **2** with CT-DNA, the intrinsic binding constant K_b was determined from the spectral titration data using the equation [62]:

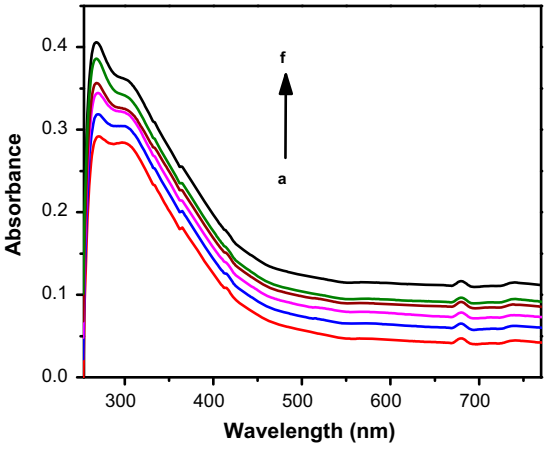

Figure 4. Electronic spectral titration of **2** with CT-DNA at 269 nm in tris–HCl buffer; [**2**] = 1.09×10^{-4}; [DNA]: (a) 0.0, (b) 1.25×10^{-6}, (c) 2.50×10^{-6}, (d) 3.75×10^{-6}, (e) 5.00×10^{-6}, and (f) 6.25×10^{-6} M L^{-1}. The arrow indicates the increase of DNA concentration.

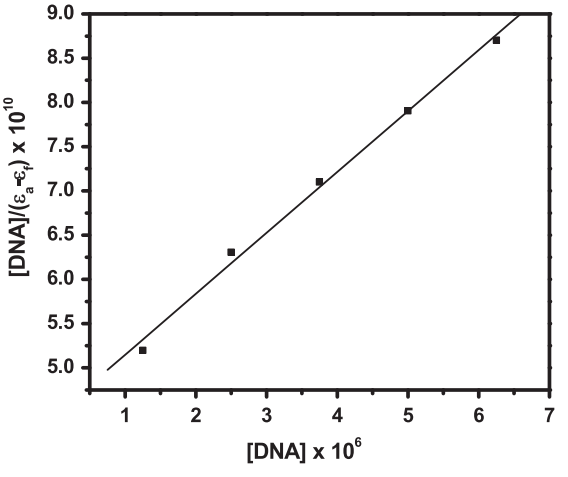

Figure 5. Plot of [DNA]/($\varepsilon_a - \varepsilon_f$) *vs.* [DNA] for the absorption of CT-DNA with **2** in tris–HCl buffer.

$$[\mathrm{DNA}]/(\varepsilon_a - \varepsilon_f) = [\mathrm{DNA}]/(\varepsilon_b - \varepsilon_f) + 1/[K_b/(\varepsilon_b - \varepsilon_f)] \quad (1)$$

where [DNA] is the concentration of DNA, ε_f, ε_a, and ε_b correspond to the extinction coefficient, respectively, for free **2**, for each addition of DNA to **2** and for **2** in fully bound form. A plot of [DNA]/($\varepsilon_a - \varepsilon_f$) *versus* [DNA], gives K_b, the intrinsic binding constant as the ratio of slope to intercept. From the [DNA]/($\varepsilon_a - \varepsilon_f$) *versus* [DNA] plot (figure 6), the binding constant K_b for **2** was estimated to be 0.31×10^5 M^{-1} ($R = 0.99478$ for five points). However, the binding constant K_b for **2** with CT-DNA was found to be lower than those observed in reported intercalative complexes [35, 63, 64], but comparable with the partial intercalant cobalt(II) complex of dimethylcantharate and 2,2′-bipyridine [65].

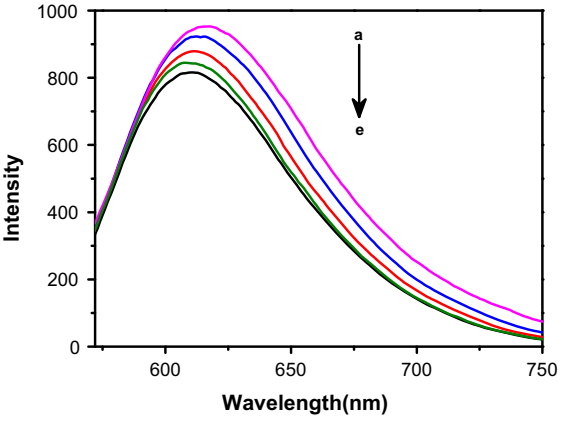

Figure 6. Emission spectra of the CT-DNA-EB system in tris–HCl buffer upon titration of **2**. $\lambda_{ex} = 522$ nm; [EB] $= 9.6 \times 10^{-5}$ M L^{-1}, [DNA] $= 1.25 \times 10^{-5}$; [Complex]: (a) 0.0, (b) 1.36×10^{-5}, (c) 2.72×10^{-5}, (d) 4.08×10^{-5}, and (e) 5.44×10^{-5} M L^{-1}. The arrow denotes the gradual increase of concentration of the complex.

3.6.2. Fluorescence quenching technique. Fluorescence intensity of EB bound to DNA at 612 nm shows a decreasing trend with increasing concentration of the compound. The quenching of EB bound to DNA by the compound is in agreement with the linear Stern–Volmer equation [66]:

$$I_0/I = 1 + K_{sv}[Q] \tag{2}$$

where I_0 and I represent the fluorescence intensities in the absence and presence of quencher, respectively. K_{sv} is a linear Stern–Volmer quenching constant and Q is the concentration of quencher. In the quenching plot in figure 6 of I_0/I *versus* **2**, K_{sv} is given by the ratio of the slope to intercept. The K_{sv} value for **2** is 0.39×10^4 ($R = 0.99746$ for five points), suggesting a strong affinity of the compound to CT-DNA.

3.6.3. Number of binding sites. Fluorescence quenching data were used to determine the binding sites (n) for **2** with CT-DNA. Figure 7 shows the fluorescence spectra of EB-DNA in the presence of different concentrations of **2**. It can be seen that the fluorescence intensity at 612 nm was used to estimate K_{sv} and n.

If it is assumed that there are similar and independent binding sites in EB-DNA, the relationship between the fluorescence intensity and the quencher medium can be deduced from equation (3):

$$nQ + B \longrightarrow Q_n \ldots B \tag{3}$$

where B is the fluorophore, Q is the quencher, $[nQ + B]$ is the postulated complex between the fluorophore and n molecules of the quencher. The constant K is given by equation (4):

$$K = [Q_n \ldots B]/[Q]^n \cdot [B] \tag{4}$$

If the overall amount of biomolecules (bound or unbound with the quencher) is B_o, then $[B_o] = [Q_n \ldots B] + [B]$, where B is the concentration of unbound biomolecules, and the

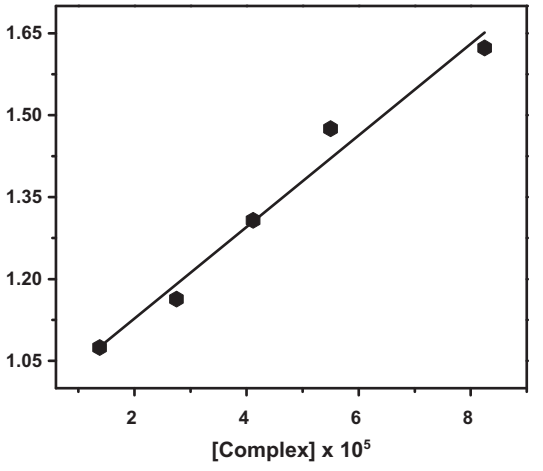

Figure 7. Plot of I_0/I *vs.* **2** for titration of CT-DNA-EB system with **2** using a spectrofluorimeter; linear Stern–Volmer quenching constant (K_{sv}) for **2** = 0.39×10^4 ($R = 0.99746$ for five points).

relationship between the fluorescence intensity and the unbound biomolecule as $[B]/[B_o] = I/I_0$, that is:

$$\log[I_0 - I] = \log K + n \log[Q] \tag{5}$$

where n is the number of binding sites of **2** with CT-DNA, which can be determined from the slope of $\log[(I_0 - I)/I]$ *versus* $\log[Q]$, as shown in figure 8. The calculated value of the number of binding sites (n) is 1.19 ($R = 0.99862$ for five points). The value of n approximately equals 1, and thus indicates the existence of just a single binding site in DNA for **2**.

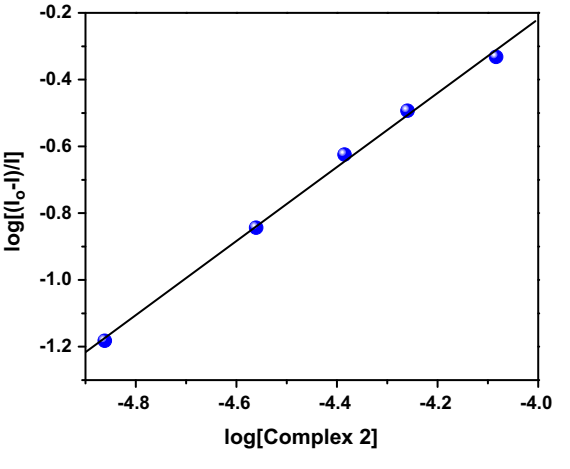

Figure 8. Plot of I_0/I *vs.* [Complex] for titration of **2** with CT-DNA-EB system in tris–HCl buffer.

3.6.4. Viscometric measurements. To obtain direct evidence of DNA interaction with **2** and specifically to discriminate between DNA intercalation and groove-binding modes, viscosity measurements were carried out. Upon binding, a DNA intercalator causes an increase in the viscosity of the DNA double helix due to its insertion between the DNA base pairs and consequently to lengthening of the DNA double helix. In contrast, a partial and/or non-classical intercalation could bend (or kink) the DNA helix, reducing the effective length and its viscosity [67]. The effect of **2** on viscosity of CT DNA is shown in figure 9. The viscosity of DNA increased dramatically upon addition of **2** and is nearly linear at low concentration region. These results strongly indicate that the imine dithiocarbamate compound intercalated deeply into the DNA base pairs.

3.7. *Binding experiments with BSA*

3.7.1. Absorption spectral technique. Absorption spectra of BSA in the absence and presence of **2** at different concentrations were recorded in DMSO-H_2O medium (figure 10). The spectra indicate a significant increase in the absorbance of BSA by increasing the concentration of the complex and are indicative of the fact that BSA adsorbs strongly the complex on its surface. From these data, the apparent association constant (K_{app}) of the complex with BSA has been determined using the following equation [68]:

$$1/(A_{obs} - A_0) = 1/(A_c - A_0) + 1/K_{app}(A_c - A_0)[\text{complex}]$$

where A_{obs} is the observed absorbance of the solution containing different concentrations of the complex at 280 nm, A_0 and A_c are the absorbances of BSA and the complex at 280 nm, respectively, with a concentration of C_0, and K_{app} represents the apparent association constant. The enhancement of absorbance at 280 nm was due to absorption of the surface complex, based on the linear relationship between $1/(A_{obs} - A_0)$ *versus* reciprocal concentration of the complex with a slope equal to $1/K_{app}(A_c - A_0)$ and an intercept equal to

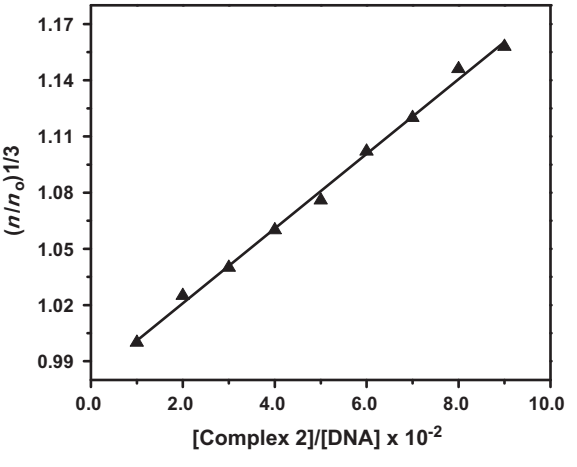

Figure 9. Viscometric experiments of CT-DNA and **2** at 25 °C (50 mM tris-buffer); assays were performed in triplicate. Slope: 1.999 ± 0.004; $R^2 = 0.99621$ for nine points.

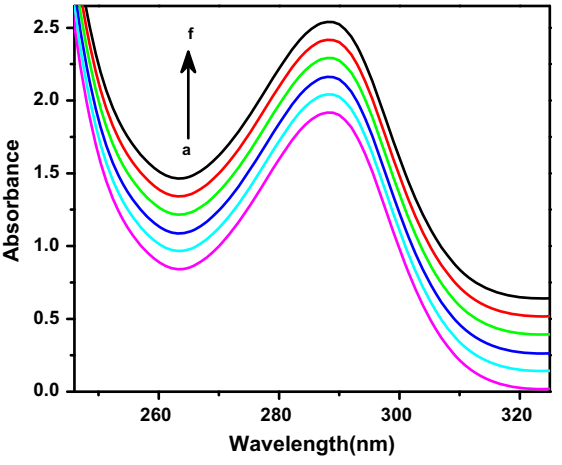

Figure 10. Absorption titration spectra of BSA in the presence of **2**. Concentration range of complex is 0–6.25 × 10^{-6} M^{-1}.

$1/(A_c - A_0)$ (figure 11). The value of the apparent association constant (K_{app}) determined from this plot is 8.4388×10^4 M^{-1} ($R = 0.99462$ for five points).

3.7.2. Fluorescence quenching. The effect of increasing the concentration of **2** on the fluorescence emission spectra of BSA were studied and is presented in figure 12. With the addition of complex, BSA fluorescence emission is quenched. The fluorescence quenching is described by the Stern–Volmer relation [60]:

$$I_0/I = 1 + K_{sv}\,[\text{complex}]$$

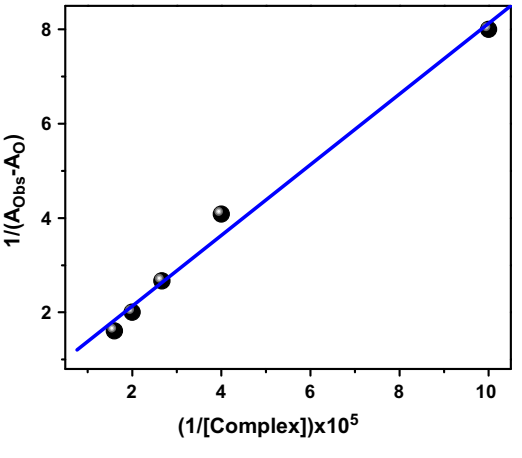

Figure 11. Linear dependence of $1/A - A_0$ on the reciprocal concentration of **2**.

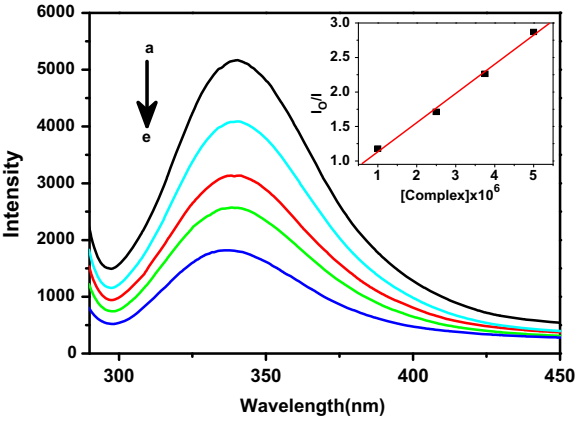

Figure 12. Fluorescence quenching titration of BSA varying the concentrations of **2**, [Complex]: (a) 0.0, (b) 1×10^{-5}, (c) 2×10^{-5}, (d) 3×10^{-5}, and (e) 4×10^{-5} M L^{-1}; inset shows the Stern–Volmer plot.

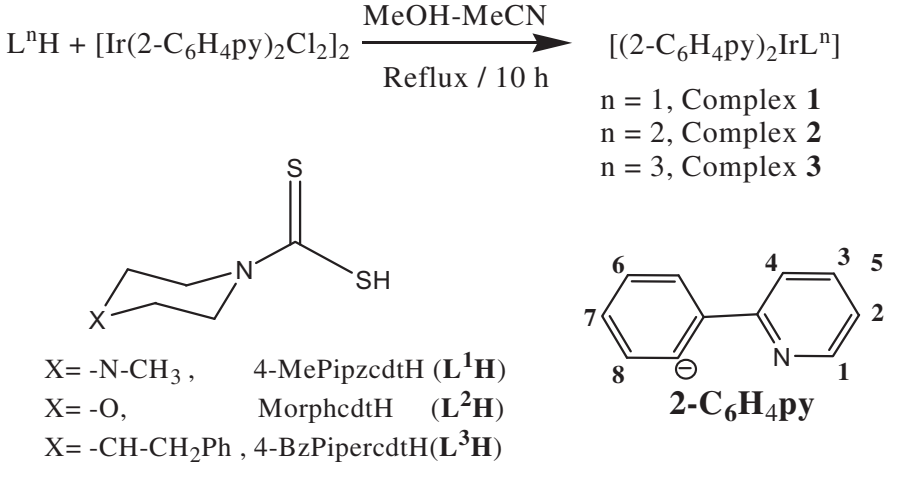

Scheme 1. Synthetic strategy of iridium(III) complexes with the corresponding ligands.

where I_0 and I represent the fluorescence intensities of BSA in the absence and presence of quencher, respectively. K_{sv} is the linear Stern–Volmer quenching constant and [complex] the molar concentration of the quencher. A linear plot (inset, figure 12) between I_0/I against [complex] was obtained, and from the slope, we calculated K_{sv} as 5.31×10^5 (R = 0.98942 for five points).

3.8. *Antibacterial activity*

Antibacterial activity of the dithiocarbamic acids (HL) and the corresponding complexes are tabulated in table 5. Comparisons of the biological activity of the dithiocarbamates and their iridium(III) derivatives with the standard antibiotic *chloramphenicol* at different

Table 5. Antibacterial data of free dithiocarbamic acids (**LH**) and **1**, **2**, and **3** (100 μg/mL).

Compound for treatment	Inhibition zone in mm			
	E. coli	*V. cholerae*	*B. cereus*	*S. pneumoniae*
$\mathbf{L^1H}$	03	03	04	02
$\mathbf{L^2H}$	04	03	07	03
$\mathbf{L^3H}$	04	06	05	03
1	07	06	05	05
2	13	15	14	13
3	08	09	09	07
Chloramphenicol	19	28	30	20
DMF	0	0	0	0

concentrations have been carried out taking usual precautions. From this study, it may be concluded that the iridium(III) complexes have higher activity than the ligand, but less efficient than the antibiotics. The increased activity may be due to increase of the delocalization of π-electrons over the whole chelate ring imparting increased lipophilic character to the metal complexes. This higher lipophilicity of the complexes facilitates the penetration ability into the bacterial cell membranes, and as result, it perturbs the respiration process of the bacteria and slows down the further growth of the micro-organisms.

4. Conclusion

Three neutral cyclometalated iridium(III) complexes bearing dithiocarbamate derivatives formulated as $[Ir(2\text{-}C_6H_4py)_2(L^1)]$ (**1**), $[Ir(2\text{-}C_6H_4py)_2(L^2)]$ (**2**), and $[Ir(2\text{-}C_6H_4py)_2(L^3)]$ (**3**) have been synthesized and characterized by solid and solution phase spectroscopic studies, including detailed structural analysis of **2** by single-crystal X-ray study. The interaction with CT-DNA shows that these cyclometalated iridium(III) complexes are good intercalators to CT-DNA with an adequate number of coordination sites. The viscometric measurement shows that **2** interacts with CT-DNA as a intercalant. The antibacterial studies suggest that all the complexes have higher activities than the free dithiocarbamic acids (LH) against four pathogenic bacteria (*E. coli*, *V. cholerae*, *S. pneumoniae*, and *B. cereus*); among these three complexes, **2** has more antibacterial effect.

Supplementary material

Crystallographic data for **2** have been deposited with the Cambridge Crystallographic Data Center, CCDC No. 932588. Copies of this information are available on request at free of charge from CCDC, 12 Union Road, Cambridge CB21EZ, UK (Fax: +44 1223 336 033; E-mail: deposit@ccdc.ac.uk or http://www.ccdc.cam.ac.uk).

Acknowledgements

Financial support from the Council of Scientific and Industrial Research (CSIR), New Delhi, India is gratefully acknowledged.

References

[1] M.A. Baldo, D.F. O'Brien, Y. You, A. Shoustikov, S. Sibley, M.E. Thompson, S.R. Forrest. *Nature*, **395**, 151 (1998).
[2] K.K.W. Lo, M.W. Louie, K.Y. Zhang. *Coord. Chem. Rev.*, **254**, 2603 (2010).
[3] Y. Chi, P.T. Chou. *Chem. Soc. Rev.*, **39**, 638 (2010).
[4] W.Y. Wong, C.L. Ho. *Coord. Chem. Rev.*, **253**, 1709 (2009).
[5] Z.Q. Chen, Z.Q. Bian, C.H. Huang. *Adv. Mater.*, **22**, 1534 (2010).
[6] C. Wu, H.F. Chen, K.T. Wong, M.E. Thompson. *J. Am. Chem. Soc.*, **132**, 3133 (2010).
[7] M. Mauro, K.C. Schuermann, R. Prétôt, A. Hafner, P. Mercandelli, A. Sironi, L. De Cola. *Angew. Chem. Int. Ed.*, **49**, 1222 (2010).
[8] L. Yu, Z. Huang, Y. Liu, M. Zhou. *J. Organomet. Chem.*, **718**, 14 (2012).
[9] R. Srivastava, Y. Kada, B. Kotamarthi. *Comput. Theor. Chem.*, **1009**, 35 (2013).
[10] J.-Y. Qiang, Y.-Q. Xu, B. Tong, X.-F. Ma, Q. Chen, W.-H. Leung, Q.-F. Zhang. *Inorg. Chim. Acta*, **394**, 184 (2013).
[11] Q. Zhao, T.Y. Cao, F.Y. Li, X.H. Li, H. Jing. *Organometallics*, **26**, 2077 (2007).
[12] Q. Zhao, S.J. Liu, F.Y. Li. *Dalton Trans.*, 3836 (2008).
[13] H.F. Shi, S.J. Liu, H.B. Sun. *Chem. Eur. J.*, **16**, 12158 (2010).
[14] Y. Liu, M.Y. Li, Q. Zhao. *Inorg. Chem.*, **50**, 5969 (2011).
[15] Y. Wu, H. Jing, Z. Dong, Q. Zhao, H. Wu, F. Li. *Inorg. Chem.*, **50**, 7412 (2011).
[16] B. Tong, Q. Mei, M. Lu. *Inorg. Chim. Acta*, **391**, 15 (2012).
[17] B. Tong, M. Zhang, Z. Han, Q. Mei, Q. Zhang. *J. Organomet. Chem.*, **724**, 180 (2013) and references therein.
[18] M. Gras, B. Therrien, G. Süss-Fink, A. Casini, F. Edafe, P.J. Dyson. *J. Organomet. Chem.*, **695**, 1119 (2010).
[19] V. Fernandez-Moreira, F.L. Thorp-Greenwood, M.P. Coogan. *Chem. Commun.*, **46**, 186 (2010).
[20] K.Y. Zhang, H.W. Liu, T.T.H. Fong, X.G. Chen, K.K.W. Lo. *Inorg. Chem.*, **49**, 5432 (2010).
[21] C. Li, M. Yu, Y. Sun, Y. Wu, C. Huang, F. Li. *J. Am. Chem. Soc.*, **133**, 11231 (2011).
[22] R. Cao, J. Jia, X. Ma, M. Zhou, H. Fei. *J. Med. Chem.*, **56**, 3636 (2013).
[23] C. Dolan, R.D. Moriarty, E. Lestini, M. Devocelle, R.J. Forster, T.E. Keyes. *J. Inorg. Biochem.*, **119**, 65 (2013).
[24] J.M. Hearn, I. Romero-Canelón, B. Qamar, Z. Liu, I. Hands-Portman, P.J. Sadler. *ACS Chem. Biol.*, **8**, 1335 (2013).
[25] K.K.-W. Lo, M.-W. Louie, K.Y. Zhang. *Coord. Chem. Rev.*, **254**, 2603 (2010).
[26] M.A. Nazif, J.A. Bangert, I. Ott, R. Gust, R. Stoll, W.S. Sheldrick. *J. Inorg. Biochem.*, **103**, 1405 (2009).
[27] M. Kokoschka, J.A. Bangert, R. Stoll, W.S. Sheldrick. *Eur. J. Inorg. Chem.*, 1507 (2010).
[28] Y.-M. Chen, A.-G. Zhang, Y.-J. Liu, K.-Z. Wang. *J. Organomet. Chem.*, **696**, 1716 (2011).
[29] A.M. Bond, R.L. Martin. *Coord. Chem. Rev.*, **54**, 23 (1984).
[30] M. Cano, J.A. Campo, P. Ovejero, J.V. Heras. *J. Organomet. Chem.*, **396**, 49 (1990).
[31] M. Bardají, A. Laguna, M. Laguna, F. Merchán. *Inorg. Chim. Acta*, **215**, 215 (1994).
[32] A.M. Bond, R. Colton, B.M. Gatehouse, Y.A. Mah. *Inorg. Chim. Acta*, **260**, 61 (1997).
[33] A. Elduque, C. Finestra, J.A. López, F.J. Lahoz, F. Merchán, L.A. Oro, M.T. Pinillos. *Inorg. Chem.*, **37**, 824 (1998).
[34] L. Chen, C. Yang, J. Qin, J. Gao, H. You, D. Ma. *J. Organomet. Chem.*, **691**, 3519 (2006).
[35] T. Mukherjee, B. Sen, A. Patra, S. Banerjee, G. Hundal, P. Chattopadhyay. *Polyhedron*, **69**, 127 (2014) and references therein.
[36] J. Chen, C. Du, J. Kang, J. Wang. *Chem. Biol. Interact.*, **171**, 26 (2008).
[37] J.K. Barton, J.M. Goldberg, C.V. Kumar, N.J. Turro. *J. Am. Chem. Soc.*, **108**, 2081 (1986).
[38] J.G.M. Gómez-Segura, M.J. Prieto, M.F. Font-Bardia, X. Solans, V. Moreno. *Inorg. Chem.*, **45**, 10031 (2006).
[39] X. Sheng, X. Guo, X.M. Lu, G.Y. Lu, Y. Shao, F. Liu, Q. Xu. *Bioconjugate Chem.*, **19**, 490 (2008).
[40] T. Mukherjee, B. Sen, E. Zangrando, G. Hundal, B. Chattopadhyay, P. Chattopadhyay. *Inorg. Chim. Acta*, **406**, 176 (2013).
[41] C. Genre, G. Levasseur-Thériault, C. Reber. *Can. J. Chem.*, **87**, 1625 (2009).
[42] T. Mukherjee, S. Sarkar, J. Marek, E. Zangrando, P. Chattopadhyay. *Transition Met. Chem.*, **37**, 155 (2012).
[43] E.L. Gelamo, M. Tabak. *Spectrochim. Acta, Part A*, **56**, 2255 (2000).
[44] A. Altomare, G. Cascarano, C. Giacovazzo, A. Guagliardi. *J. Appl. Crystallogr.*, **26**, 343 (1993).
[45] G.M. Sheldrick. *Acta Cryst. A*, **64**, 112 (2008).
[46] L.J. Farrugia. *J. Appl. Cryst.*, **32**, 837 (1999).
[47] S. Dey, S. Sarkar, H. Paul, E. Zangrando, P. Chattopadhyay. *Polyhedron*, **29**, 1583 (2010).
[48] C. Sheikh, M.S. Hossain, M.S. Easmin, M.S. Islam, M. Rashid. *Biol. Pharm. Bull.*, **27**, 710 (2004).
[49] S. Shivhare, D.G. Mangla. *J. Curr. Pharm. Res.*, **6**, 16 (2011).
[50] S. Basu, S. Dutta, M.G.B. Drew, S. Bhattacharya. *J. Organomet. Chem.*, **691**, 3581 (2006) and references therein.
[51] M.-K. Lau, K.-M. Cheung, Q.-F. Zhang, Y. Song, W.-T. Wong, I.D. Williams, W.-H. Leung. *J. Organomet. Chem.*, **689**, 2401 (2004).

[52] C.L. Raston, A.H. White. *J. Chem. Soc., Dalton Trans.*, 2422 (1975).
[53] F. Bonati, R. Ugo. *J. Organomet. Chem.*, **10**, 257 (1967).
[54] Y. You, S. Cho, W. Nam. *Inorg. Chem.*, **53**, 1804 (2014) and references therein.
[55] J.Y. Qiang, Y.Q. Xu, B. Tong, X.F. Ma, Q. Chen, W.H. Leung, Q.F. Zhang. *Inorg. Chim. Acta*, **394**, 184 (2013) and references therein.
[56] P.J. Hay. *J. Phys. Chem. A*, **106**, 1634 (2002).
[57] C. Chen, X. Qi, B. Zhou. *J. Photochem. Photobiol. A: Chem.*, **109**, 155 (1997).
[58] K. Dhara, J. Ratha, M. Manassero, X.Y. Wang, S. Gao, P. Banerjee. *J. Inorg. Biochem.*, **101**, 95 (2007).
[59] K. Dhara, P. Roy, J. Ratha, M. Manassero, P. Banerjee. *Polyhedron*, **26**, 4509 (2007).
[60] V.A. Bloomfield, D.M. Crothers, I. Tinoco. *Physical Chemistry of Nucleic Acids*, p. 432, Harper and Row, New York (1974).
[61] A. Ambroise, B.G. Maiya. *Inorg. Chem.*, **39**, 4264 (2000).
[62] S.A. Tysoe, R.J. Morgan, A.D. Baker, T.C. Strekas. *J. Phys. Chem.*, **97**, 1707 (1993).
[63] T.-T. Xing, S.-H. Zhan, Y.-T. Li, Z.-Y. Wu, C.-W. Yan. *J. Coord. Chem.*, **66**, 3149 (2013).
[64] H. Paul, T. Mukherjee, M. Mukherjee, T.K. Mondal, A. Moirangthem, A. Basu, E. Zangrando, P. Chattopadhyay. *J. Coord. Chem.*, **66**, 2747 (2013).
[65] F. Zhang, Q.-Y. Lin, W.-D. Liu, P.-P. Wang, W.-J. Song, B.-W. Zheng. *J. Coord. Chem.*, **66**, 2297 (2013).
[66] O. Stern, M. Volmer. *Z. Phys.*, **20**, 183 (1919).
[67] S. Satyanarayana, J.C. Dabrowiak, J.B. Chaires. *Biochemistry*, **31**, 9319 (1992).
[68] A.M. Pyle, J.P. Rehmann, R. Meshoyrer, C.V. Kumar, N.J. Turro, J.K. Barton. *J. Am. Chem. Soc.*, **111**, 3051 (1989).